מכון ויצמן למדע

WEIZMANN INSTITUTE OF SCIENCE

Thesis for the degree
Master of Science

חבור לשם קבלת התואר
מוסמך למדעים

By
Valery Garmider

מאת
ולרי גרמידר

ספקטרוסקופיה אופטית של אקסיטונים דיפוליים בבורות קוונטיים מצומדים

Optical Studies of Indirect Excitons in Coupled Quantum Wells.

Advisor
Israel Bar-Joseph

מנחה
ישראל בר יוסף

March 2008

אדר א' התשס"ח

Submitted to the Scientific Council of the
Weizmann Institute of Science
Rehovot, Israel

מוגש למועצה המדעית של
מכון ויצמן למדע
רחובות, ישראל

Abstract

Two dimensional system of indirect excitons in coupled quantum wells is a promising candidate for being a model of many interacting bosons. In the current work we investigate the problem of forming a stable gas of indirect excitons. In the first part we report experimental results indicating that above a certain density the system appears in a phase of free electrons and holes rather than in a form of electron-hole pairs bound in excitons. This is interpreted as a Mott metal to insulator transition. In the second part of this work we suggest an approach that could allow a good control of the density, temperature and lifetime of an exciton gas. The approach is based on spatial manipulation of photo-excited carriers and excitons in the plane of the quantum wells.

Table of contents

Introduction

Indirect excitons in Coupled Quantum Wells (CQW)

Molecular Beam Epitaxy (MBE) technique makes possible the fabrication of quantum confined structures with nearly any desired geometrical design in the growth direction. In the recent years, special attention has been drawn to a heterostructure constituted of two Quantum Wells (QW) separated by a tiny barrier. The band diagram of this structure is depicted in Fig. 1a. Also shown are the lowest confinement energies of the carriers in the QWs. In that particular case one of the wells is wider than the other, so the confinement energies in the wide well are smaller than those in the narrow well. The energy configuration can be further controlled by the application of electric field in the growth direction. As a result the band diagram is tilted as shown in Fig. 1b. Now consider the sample is exposed to laser radiation. If the energy of incident photons $h\nu$ is chosen to be above the energy gap of the wide well but below that of the narrow well carriers are generated in the wide well only. In addition, by a plausible choice of the electric field strength the electron confinement energy in the wide well can be tuned to be above that in the narrow well. In that configuration the electrons tunnel to the narrow well and complete charge separation in adjacent QWs is attained (Fig. 1c).

If the tunneling barrier is thin enough, spatially separated electrons and holes form the so called Indirect Excitons (IX), i.e. bound pairs of electrons and holes residing in adjacent QWs. These unique quasiparticles have the following important properties with respect to the ordinary direct excitons (X):

1. *Permanent electric dipole moment:* since the constituent electron and hole of the IX are oppositely charged and are separated by a finite distance in the growth direction, a dipole moment oriented perpendicular to the QWs is defined. One can roughly estimate its magnitude by a product of electron charge and the distance between the two QW centers: $P = e \cdot d$. The association of a dipole moment with IX implies a specific behavior of the latter when the electric field is applied perpendicular to the QWs. Its energy dependence on the field strength, *F,* is described by the dipole-field interaction: $E = -F \cdot P$ and manifests itself in a redshift of the IX

luminescence line that is *directly proportional* to the increase of the field strength [1]. The fact that Indirect Excitons carry a dipole moment leads to important consequences when a system of many interacting IXs is considered, as will be discussed in the next section. Finally IX's dipole moment makes applicable the variety of manipulation tools which will be discussed later.

2. *Long radiative recombination time:* more precise meaning of the spatial separation is that the wavepackets of the electron and the hole are concentrated in adjacent wells; hence their spatial overlap integral is significantly smaller than in the case of direct exciton where the two wavepackets are concentrated in the same well. The electron-hole recombination rate is proportional to the squared modulus of this overlap integral [2], and is reduced by orders of magnitude with respect to the direct exciton case. Hence the lifetime being the reciprocal of the recombination rate is significantly larger [3].

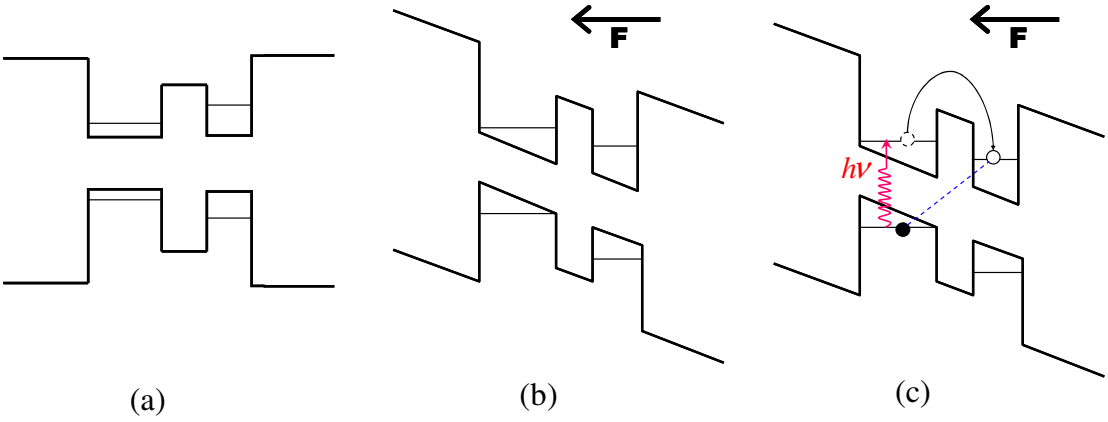

Fig 1: (a) band diagram of CQW. (b) The effect of the electric field aligned in the growth direction. (c) Carrier excitation with the subsequent tunneling and formation of Indirect Exciton marked by blue dashed line.

Two dimensional system of many IXs and its possible phases

An experimental realization of a system of many interacting particles in thermodynamic equilibrium is a necessary step towards the observation of various effects proposed theoretically. A gas of Indirect Excitons is a good starting point due to its properties described above. The lifetime of IX (lifetimes of microseconds have been reported) can be made orders of magnitude longer than the relevant time needed for the initially hot photogenerated excitons to equilibrate and reach the temperature of the lattice. The permanent dipole moment of indirect excitons causes them to repel each other due to the dipole-dipole interaction and thus prevents the formation of e-h complexes such as excitonic molecules and drops, so that pure exciton gas is assured. Furthermore, this repulsive interaction can be important if quantum phase transitions of interacting bosons are to be considered. Among the predicted theoretically interesting phases and transitions between them are the Bose-Einstein Condensate (BEC), Kosterlitz-Thouless Superfluid (KTS) [4] and exciton crystallization [5]. Special attention should be given to the Mott metal to insulator transition which is concurrent to the aforementioned phase transitions since it is expected to occur in similar experimental configuration.

N. F. Mott was concerned in the early 1960s with the problem of metal to insulator transition [6]. He proposed the following scenario as describing the phenomena: Consider a crystal lattice constituted of atoms initially positioned far away from each other. At this stage the electrons are bound to their ions inside each atom and therefore can't contribute to the conduction, i.e. the structure is an insulator. Now, suppose the distance between neighboring atoms is being reduced continuously. Then the overlap of electronic wavefunctions at adjacent atoms becomes larger while the attraction of each electron towards its respective ion gets smaller since the screening of the attraction potential due to the neighboring electrons increases. At the final stage the electrons cease to be bound to a particular ion, their wavefunction spreads all over the crystal so they are now free to move through the ionic lattice. A metallic structure is thus obtained.

In many respects a system of electrons and holes bound in excitons is similar to the lattice of electrons bound to ions described above, with one only difference: in the exciton case both electrons and holes are free to move whereas in the Mott's scenario

the ions are pinned to the lattice sites. Following the same logic, as the mean distance between the excitons is being continuously reduced, i.e. the density of excitons is increased, the mutual attraction between the electron and the hole inside a given exciton is being screened stronger and stronger, so that at some high enough density the excitons ionize and free electrons and holes are released.

The exciton Mott transition is a subject of controversies both in theory and experiment. First experimental investigations were performed on indirect gap semiconductors like Si and Ge [7]. In these works excitons with recombination times of microseconds were excited in the bulk. This lifetime is long enough for sufficient relaxation to equilibrium. However, the system was contaminated by excitonic complexes such as trions, biexcitons, etc. Their recombination spectra overlapped with those due to both exciton and electron-hole plasma, making the data difficult for interpretation. Furthermore, experiments in the bulk are problematic when homogeneous excitation is required: the finite absorption coefficient of the sample gives rise to non-uniform illumination at different depths below the surface. This prevents obtaining well defined exciton density [8]. In experiment done with QWs by Kappei et al, a clear separation of excitonic and free electron-hole luminescence was achieved providing information on Mott transition. The transition appeared rather gradual. It was attributed to the short exciton lifetime preventing equilibration. On the other hand time resolved measurement were performed by Amo et al in a bulk sample. They varied the excitation density and observed different behavior below and above certain critical temperature of the luminescence rise-time. This was claimed to indicate the Mott transition which appeared abrupt [9]. A sharp phase transition has been reported by Timofeev et al in a system of indirect excitons in CQWs [10]. This was called a "transition from a gas phase to a 2D liquid phase" but can be regarded as Mott transition in many respects.

In fact, also from the theoretical point of view it is unclear whether the transition occurs abruptly or gradually when the exciton density is continuously changed. Ben-Tabou and Laikhtman [11] followed the logic of two free-energy minima: at low temperature the number of free carriers is small and the screening of the Coulomb attraction is negligible, hence the state where most of the carriers are bound in excitons is stable. At high temperature the number of free carriers is excessively large

diminishing the binding energy by strong screening and the state where substantial amount of carriers are free is stable. Hence, the transition is characterized by a sudden jump of the system between the two potential minima at some critical temperature. Koch et al [12] have suggested an alternative mechanism to that of unbinding electron-hole pairs: the number of excitons decreases gradually but the binding of remaining excitons appears unchanged since the system rearranges itself in a configuration where the excitons are insensitive to other particles. Accordingly the transition should be a continuous one.

Spatial control of photoexcited particles in CQWs

An important aspect of studying many excitons system in QWs is the ability to manipulate and control their spatial distribution. Trapping of excitons is in particular important since it is a necessary step towards BEC in two dimensions [13]. Therefore several groups have employed various techniques of trapping. Snoke et al. [14] established a *strain induced trap*. In this method, a mechanical force is applied on a sample with a tip pin. This shifts locally the conduction band towards lower energies, thus creating an effective harmonic potential for indirect excitons. This technique has been implemented for trapping excitons [14] and polaritons [15]. Another approach is an *electrostatic potential trap*. In this set up metallic electrodes are defined on the sample surface and a voltage is applied between them and the back electrode. Thus, non-uniform electrostatic field is induced in the space where the QWs are located. The indirect excitons will tend to concentrate in the region where the out-of-plane component of the field is the highest due to the dipole-field interaction. By suitably designing the electrodes' geometry and voltage configuration an effective confining potential for indirect excitons can be established [16-17].

When a strong enough electric field is applied inside a semiconductor, the photo generated electrons and holes are more likely to be separated rather than bound into excitons, i.e., excitons are ionized by the field. The increase of the ionization rate due to the field manifests itself in the broadening of the exciton luminescence spectral line [18]. The field strength for which the effect becomes important (i.e. the threshold) is roughly $Ry/e \cdot a_B$ where *Ry* is the rydberg energy of the exciton and a_B is its Bohr

radius. Thus, taking typical values $Ry \approx 10\text{meV}$ and $a_B \approx 10\text{nm}$ we obtain $\sim 10^4$ V/cm.

When we consider excitons in quantum wells, we have to distinguish the cases of fields parallel and perpendicular to the QW plane. Since a confinement is imposed in the out-of-plane direction, the ionization is inhibited in the latter case. Rather, a quadratic dependence of the energy on the applied field, known as a quantum-confined Stark effect is obtained [18]. In the coupled quantum wells system the perpendicular field separates the oppositely charged carriers between the adjacent QWs, and in particular enables the formation of indirect excitons.

Electric field which is applied in the plane of the QW can be used to spatially manipulate the photo-excited carriers. Consider two metallic electrodes defined on the sample surface separated by a few μm from each other. If a voltage of few volts is applied between the electrodes, an electric field of $\sim 10^4$ V/cm will be induced in the space separating the electrodes and a few tens of nm under the sample surface, where the QWs are located. This field strength is enough to effectively ionize the excitons generated by a pulse of light; furthermore, the obtained electrons and holes accumulate underneath the adjacent electrodes. The large spatial separation of carriers inhibits their recombination so they are stored there as long as the voltage is applied. After the voltage is turned off, electrons and holes approach each other driven by their mutual attraction and eventually recombine releasing a pulse of light. This idea has been implemented mainly by the group of Kotthaus [19]. Storage times of milliseconds are attained limited only by carrier leakage out of the QW to the electrodes.

In the preceding paragraph we described how to temporally separate the illuminated light pulse from the luminescence light pulse. But in that set-up the photo-generated carriers are created in the same location as the light reemitted later by recombined carriers, i.e. in the gap between the electrodes. One can change this and separate these two processes spatially. Interesting approach is due to Kotthaus et al [19]. In their setup the electrons and holes are separated by a piezoelectric potential modulation induced by traveling surface acoustic wave. This potential acts as a "conveyor belt" for the carriers, since the electrons and the holes "ride" on the

potential maxima and minima with sound velocity over macroscopic distances limited only by the sample size. The potential modulation is screened by a metallic stripe located away from the illumination spot. There the carriers recombine and produce light.

In this work we shall show how these tools can be used to produce a dense and cold exciton gas.

1. The Mott transition of excitons in coupled quantum wells

This part is devoted to the problem of the Mott transition of indirect excitons in coupled quantum wells and is summarized in a paper submitted for publication. In that work we describe how the two phases, namely bound excitons and free electron-hole plasma, can be characterized and distinguished utilizing different approaches: one by means of lineshape analysis, the other involves measurements in magnetic fields. Then we establish phase diagrams of all the measured characteristic parameters in the temperature-density space. The paper concludes with the proposed model of the observed phase transition.

The Mott transition of excitons in coupled quantum wells

M. Stern,* V. Garmider, V. Umansky, and I. Bar-Joseph

Department of Condensed Matter Physics,

The Weizmann Institute of Science, Rehovot, Israel

(Dated: November 2, 2007)

Abstract

In this work we study the phase diagram of indirect excitons in coupled quantum wells , and show that the system undergoes a phase transition to unbound electron-hole plasma. This transition is manifested as an abrupt change in the photoluminescence linewidth and peak energy at some critical power density and temperature. By measuring the exciton diamagnetism, we show that the transition is associated with an abrupt increase in exciton radius. We find that the transition is stimulated by the presence of direct excitons in one of the wells, and show that they serve as a catalyst of the transition.

PACS numbers: 71.35.Lk, 78.67.De, 73.21.Fg

Interacting electrons and holes in semiconductors may form a hydrogen-like bound state, known as exciton. Its large diameter, small binding energy and strong interaction with light make it a convenient test bed for studying interaction effects in many body systems. Theoretical studies have predicted a wealth of phases for this system, with thermodynamic or quantum transitions between these phases [1]. In that context, the exciton Mott transition [2] stands as one of the puzzles of the field. At low temperature, most of the electrons and holes should be bound in excitons. As the density (or temperature) increases more and more excitons ionize, releasing free carriers. The free carriers screen the Coulomb interaction that binds the remaining excitons, facilitating their ionization. Further increase of the density (temperature) leads to avalanche ionization. This thermodynamic transition, which is also called the "ionization catastrophe" [3], has attracted a lot of attention and controversy in the past several decades. Indeed, conflicting theoretical predictions have been recently published, with some predicting an abrupt phase transition at a critical temperature or density [4], while others argue that there should be a gradual transition [5]. The experimental data seem to reflect this controversy: while the experiment of Kappei *et al.* in GaAs quantum wells shows a gradual transition [6], Amo *et al.* provide evidence for an abrupt transition in bulk GaAs [7].

Indirect excitons (IX) in coupled quantum wells (CQW) offer a unique opportunity to revisit this long standing problem. These excitons are formed by electrons and holes that reside in different quantum wells (QWs), separated by a thin tunnel barrier. Their close proximity allows them to interact and form a bound state. This unique structure gives rise to far reaching consequences. In particular, the IX lifetime can be made very long, as long as microseconds, limited only by the exponentially small overlap of the e-h wavefunctions [8]. This lifetime is much longer than the relaxation time with the thermal bath of the lattice [9–11] and the exciton formation time [12–16] and thus allows to establish a thermodynamic equilibrium, alleviating a central problem in direct excitons experiments.

In this work we study the phase diagram of optically generated IX in a CQW system, and show that it undergoes a phase transition to unbound electron-hole plasma. This transition is manifested as an abrupt change in the photoluminescence (PL) linewidth and peak energy at some critical power density and temperature. By measuring the exciton diamagnetism, we show that the transition is associated with an abrupt increase in exciton radius, from 20 nm below the critical density to > 50 nm above it. We find that the transition is stimulated

by the presence of direct excitons in one of the wells, and show that they serve as a catalyst of the transition. Indeed, we find that in the absence of these catalysts the phase transition is not observed.

The sample that we investigated is an n^+- i- n^+ structure grown by molecular beam epitaxy on semi-insulating GaAs substrate. The i-region consists of two GaAs quantum wells of different width, 7 and 10 nm, separated by 5 nm $Al_{0.28}GaAs$ barrier and surrounded by two AlGaAs spacer layers. An electric field $F = 24$ kV/cm was applied in a direction perpendicular to the QWs, such that the electron level in the wide well is higher than that of the narrow well. Changing the strength of this field modifies the e-h overlap integral and therefore the carrier's recombination time. Hence, the main effect of varying the field is changing the e-h pair's density in steady state. To perform the PL measurements we prepared a large area sample (1.5 mm^2). The mesa was illuminated by a laser spot which covered approximately a quarter of the area, and the PL was collected from a small spot of a few tens of microns in diameter. This ensures that the exciton density in the area from which we collect the PL is uniform.

The samples were excited using a tunable Ti:Sapphire laser. By selecting the excitation energy E_L to be above or below the narrow well gap, E_{NW}, we could select two different initial conditions. At $E_L < E_{NW}$ electrons and holes are excited in the wide well only. The electrons quickly tunnel into the narrow well and at steady state one gets nearly complete charge separation: the electrons reside in the narrow well while the holes are in the wide well. The only excitons that are observed under this condition are indirect ones. This is changed when $E_L > E_{NW}$, when electrons and holes are created at both wells. Here also the electrons would tunnel into the narrow well. However, the tunneling time of the holes is much longer and we get a population of holes trapped at the narrow well. As a consequence we get a mixture of two types of excitons: indirect and direct ones, the latter being formed between electrons and holes in the narrow well. We shall see that this difference has far reaching implications on the nature of the transition. We note that in both cases the excitation energy is well below the $Al_{0.28}GaAs$ gap, thus the leakage current is significantly reduced relative to the recently reported He-Ne experiments [17–19]: a typical value is 250 $\mu A/cm^2$ at excitation power of 1 W/cm^2 and electric field of 24 kV/cm.We verified that the accumulation of extra charges in the QWs, originating from shallow impurities in the spacer, is negligible [20].

Let us begin with the case of $E_L < E_{NW}$ at $T = 1.5$ K, where only indirect excitons

can be formed. The binding energy of the indirect excitons is $E_B = 2.5$ meV, 20 times larger than k_BT at that temperature. Hence, the number of ionized excitons is expected to be negligibly small, suppressed by a factor of $\exp\left(\frac{-E_B}{k_BT}\right)$ relative to the bound ones. Indeed, the PL measurements show that the carriers are bound in excitons even at very high densities (Fig. 1). In Fig. 1a, we show the PL energy as a function of power density. We observe a relatively small blueshift of 0.6 meV as the power density is increased up to 4 W/cm^2. The origin of this blueshift is the interaction between the excitons, which have a permanent dipole along the growth direction, and, thus, exercise a repulsive force on each other. Using the recent calculations of Zimmermann [21] one can estimate the exciton density that corresponds to the observed blue-shift to be 6×10^{10} cm$^{-2.}$ This density is comparable with the so-called Mott density $1/a_B$, where a_B is the exciton Bohr radius, yet no transition is observed. The presence of a high exciton density is also manifested in the PL spectrum: the linewidth increases by 50%, from 1 to 1.5 meV over this density range (Fig. 1b), while the integrated intensity grows precisely linearly with power.

To get a deeper insight into the nature of the excited system we measured the behavior of the PL energy as a function of magnetic field B, applied in Faraday configuration. It is well known that the exciton ground state energy should increase quadratically with magnetic field, a phenomenon known as the exciton diamagnetic shift [22]. The shift is given by $\Delta E(B) = \alpha B^2 \langle r^2 \rangle$, where $\langle r^2 \rangle$ is the expectation value of the exciton radius squared, $\alpha = \frac{e^2}{8\mu c^2}$, and μ is the reduced mass of the exciton in the plane parallel to the QWs. This is in contrast to uncorrelated e-h plasma, which exhibit a linear dependence of the energy on B, given by $\Delta E(B) = \hbar\omega_c/2$, where ω_c is the cyclotron frequency. This measurement allows us to distinguish between excitons and plasma, and to determine the expectation value of the exciton radius $\sqrt{\langle r^2 \rangle}$. The inset of Fig. 1c shows a typical measurement of PL energy dependence on B. A clear parabolic dispersion is seen throughout this density range, supporting the conclusion that the carriers are bound and form excitons. We find that the diamagnetism *decreases* with increasing exciton density, indicating that the exciton radius becomes smaller at high density. This is in clear contrast with the naive Mott scenario, where the excitons are expected to be less bound as the density increases.

Let us turn now into the second case of $E_L > E_{NW}$, where we get a mixture of direct and indirect excitons. We find that the dependence of PL on power density is radically different, and an abrupt change is found at 0.75 W/cm^2. Figure 2a shows the change of the linewidth

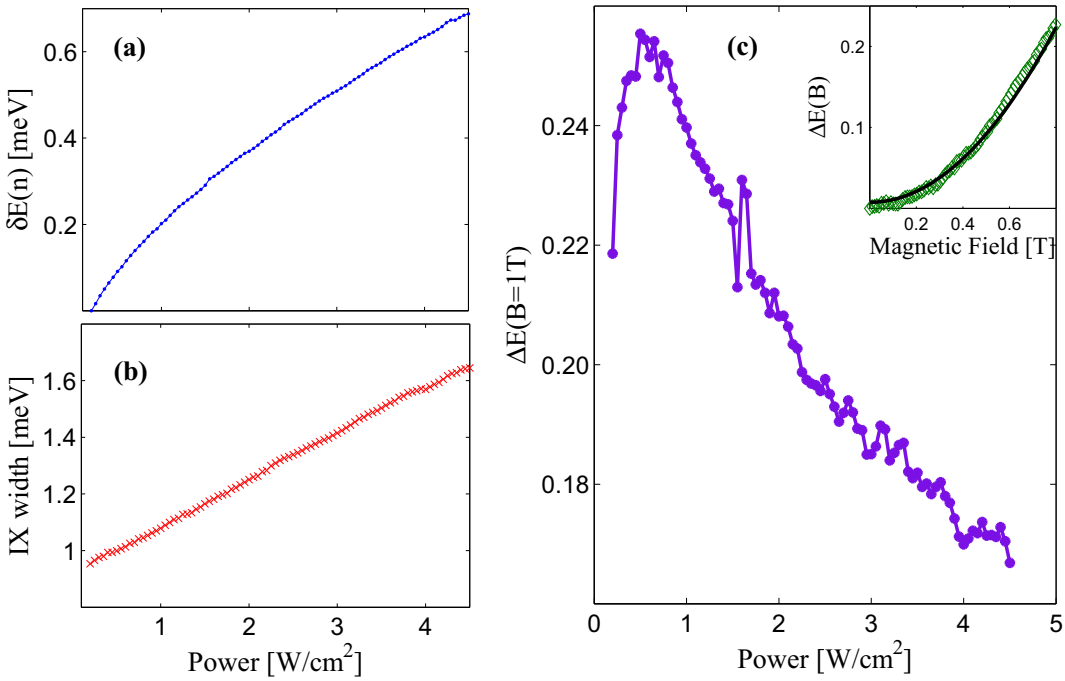

FIG. 1: The PL properties for excitation in the wide well only $E_L < E_{NW}$ T= 1.5 K . (a) The PL energy shift, (b) the linewidth and (c) the diamagnetic coefficient of the IX peak as a function of power density. Inset of (c): Quadratic behavior of the peak energy as function of magnetic field.

near the transition: an abrupt change from a width of 1 meV below the transition to 1.2 meV above it is seen. It is interesting to note that the transition is accompanied by a modification of the lineshape from being predominantly Lorentzian at low power densities to Gaussian at high densities. The transition is extremely abrupt and can not be resolved within our power resolution (0.1 mW/cm^2). Figure 2b shows a close-up view of the behavior of the PL energy versus power near the transition point: it can be clearly seen that the slope of the curve abruptly changes from shallow to steep. To understand the origin of this behavior let us consider the density dependence of the PL energy in two limits, uncorrelated e-h plasma and an exciton gas. In the e-h plasma regime the separation of charges in the two wells creates an electric field which screens out the external electric field and shifts the recombination

energy to higher values. The blueshift of the PL energy can be straightforwardly calculated as $\delta E(n) = \frac{4\pi e^2 d}{\varepsilon} n$, where n is the density of the uncorrelated e-h pairs, d is the separation between the centers of the two wells and ε is the dielectric constant. On the other hand, at the excitonic regime the energy shift is primarily due to the repulsive interaction [21] between the excitons, as discussed earlier. In a simplified picture, each exciton creates a depletion region around itself and as a consequence the blueshift is temperature dependent and much weakerthe than in the uncorrelated case. The blueshift based estimate of the exciton density at the transition [21] is 2×10^{10} cm^{-2} at 1.8 K. To confirm this estimate we performed PL measurements at magnetic fields and determined the magnetic field at which the lowest Landau level (LL) is full. At this magnetic field the PL from the second LL is diminished. This measurement can be conducted only at high carrier densities, well above the transition. We find that the carrier density depends linearly on power, and we could therefore extrapolate the linear dependence to extract the density at the transition. This estimate agrees very well with that based on the blueshift.

Here again we obtain a deeper insight by measuring the diamagnetic behavior. Figure 2c shows the PL energy as a function of magnetic field for two power densities, below and above the transition. One can clearly see how the quadratic behavior at low power densities turns into almost linear at high power. The in-plane radius of the indirect excitons at low power can be readily extracted from this measurement and found to be ~ 20 nm. Applying this analysis to the high power data yields a lower bound of 50 nm for the exciton radius. We verified the validity of this approach by comparing it to the diamagnetic shift of the direct exciton, which is found to yield the expected radius of ~ 10 nm. This clearly indicates that the transition is accompanied by a substantial change of exciton size, from being bound to unbound. Figure 2d shows the diamagnetic coefficient as a function of power density. Two regimes of diamagnetism are clearly observed, with a sharp boundary between a phase of bound excitons and a phase of unbound e-h pairs. It is interesting to note that we do not observe a gradual increase of the exciton radius below the transition as implied by the Mott transition scenario.

To establish the fact that this is indeed a thermodynamic phase transition we measured the temperature dependence of the transition. Figure 3a shows the evolution of the PL linewidth and blueshift with temperature at $P = 0.95$ W/cm^2. We find that at low temperatures ($T = 1.6$ K) the linewidth is broad and reaches 1.8 meV, characteristic of unbound

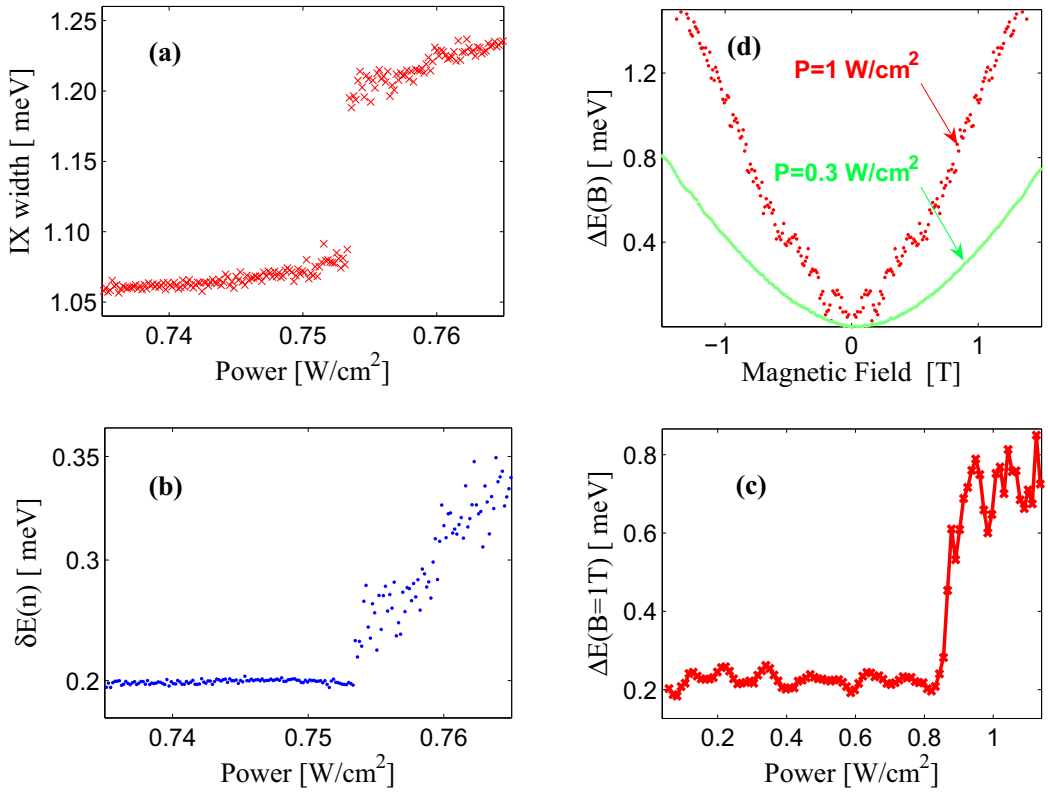

FIG. 2: The PL properties for excitation in both wells, $E_L > E_{NW}$ T= 1.5 K. (a) The linewidth, (b) the PL energy shift and (c) the diamagnetic coefficient as function of power density. (d) The diamagnetic shift at two power levels, below and above the transition. The magnetic field dependence measurements were conducted in a different cryostat with fiber illumination.

electron-hole plasma. As the temperature is increased the width decreases rapidly and levels at 1.3 meV above 3K. Upon further increase of the temperature we observe an opposite transition above 6 K – the PL linewidth turns from excitonic to e-h plasma. The same re-entrance behavior is observed when examining the blueshift of the PL energy. The phase diagram in the power-temperature $(P-T)$ plane is depicted in Fig. 3b (the dashed line describes the measurement of Fig. 3a). One can see that the excitonic phase indeed exists only in a limited area in this parameter space.

Our results clearly show that in the case of a mixed X and IX phase an abrupt thermodynamic phase transition takes place, between bound to unbound e-h. A natural question

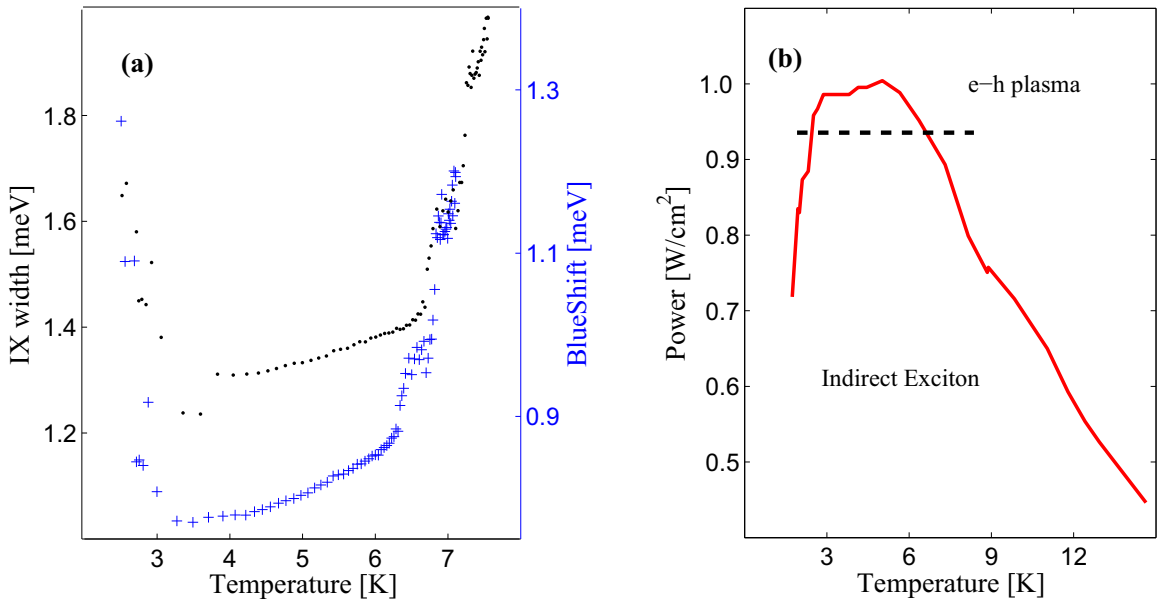

FIG. 3: (a) The linewidth (points) and blueshift (crosses) as function of temperature for $P = 0.95$ W/cm^2. (b) Power-temperature phase diagram showing the IX and e-h regions. The dashed line corresponds to the parameters of (a).

to ask is what is the underlying mechanism that distinguishes this system and gives rise to the observed behavior. An insight into the origin of this mechanism is obtained by carefully examining the changes in the direct exciton luminescence. We find that at the phase transition threshold a new line appears 2.1 meV below the narrow well X line (Fig. 4a), and its intensity increases linearly at higher powers. By examining its behavior in electric and magnetic field we could unambiguously identify it as the narrow well trion, T, a bound state of two electrons and a hole [23, 24].

To understand the implications of this observation we should recall that the carriers are arranged such that all electrons reside in the narrow well while the holes are divided between the two wells. At low densities the holes in the narrow well bind to the electrons in that

well and form direct excitons, X. The remaining electrons bind with the holes in the other well and form indirect excitons, IX, gaining 2.5 meV of binding energy. However, there is another possible channel for these electrons, and that is to bind to an exciton and form a trion, T, gaining only 2.1 meV. This is clearly a higher energy state and, therefore, the system prefers the $IX + X$ state as its ground state (Fig. 4c). However, the T state is only 0.4 meV higher, which is $2 - 3\ k_B T$ above in the temperature range of the experiment, and a substantial portion of the IX ionizes to T through the process $IX + X \longrightarrow T + h$. Since their lifetime is very short, the trions recombine quickly and leave behind free electrons. Unlike the pure IX case, where the ionization level is a binding energy above, we have here an efficient channel of ionizing the IX which is only a few $k_B T$ higher than the ground state. This allows us to set the necessary conditions for the ionization catastrophe to occur, and reproduce the conditions for the Mott transition to be observed.

In the concluding part of this paper we wish to return to the $P - T$ phase diagram and suggest a qualitative explanation for its unique shape. Let us consider two states of the system: a bound exciton gas and a pure free e-h plasma. If we assume that the screening of the excitonic interaction is due to the free e-h, and that it can be treated within the Thomas Fermi approximation, we may write the free energy per particle of the exciton system as $f_X = U_B\left(l/a_B\right) - s_x T$, where U_B is the screened binding potential, l is the screening length and s_x is the entropy. In the Thomas Fermi approximation $l = \frac{2\varepsilon k_B T}{e^2 n}$where n is the free e-h density, and $-R_y \leq U_B \leq 0$ for $1/2 \leq l/a_B \leq \infty$. The blue line in Fig. 4b shows some generic dependence of U_B on l, or equivalently on T/n. In the other limit of e-h plasma the free energy can be written simply as $f_{e-h} = -s_{e-h} T$. The ground state of the system can therefore be determined by comparing f_X and f_{e-h}, and the transition line is determined by solving $f_X - f_{e-h} = 0$. A graphical solution is provided in Fig. 4b for several values of free e-h pairs n_1, n_2 and n_3 (for the sake of clarity $s_X T$ was substracted from f_X and was added to f_{e-h}). It is seen that this equation has two solutions for a wide range of values, and no solution beyond a certain value, as indeed observed experimentally. While this model provides a qualitative understanding of the transition it is very simplified: it considers the exciton screening within a simple approximation and neglects changes in the exciton distribution [5] which should modify the system's entropy. Furthermore, it neglects interaction effects and band gap renormalization in the e-h plasma. These require a more detailed analysis which is beyond the scope of the current paper.

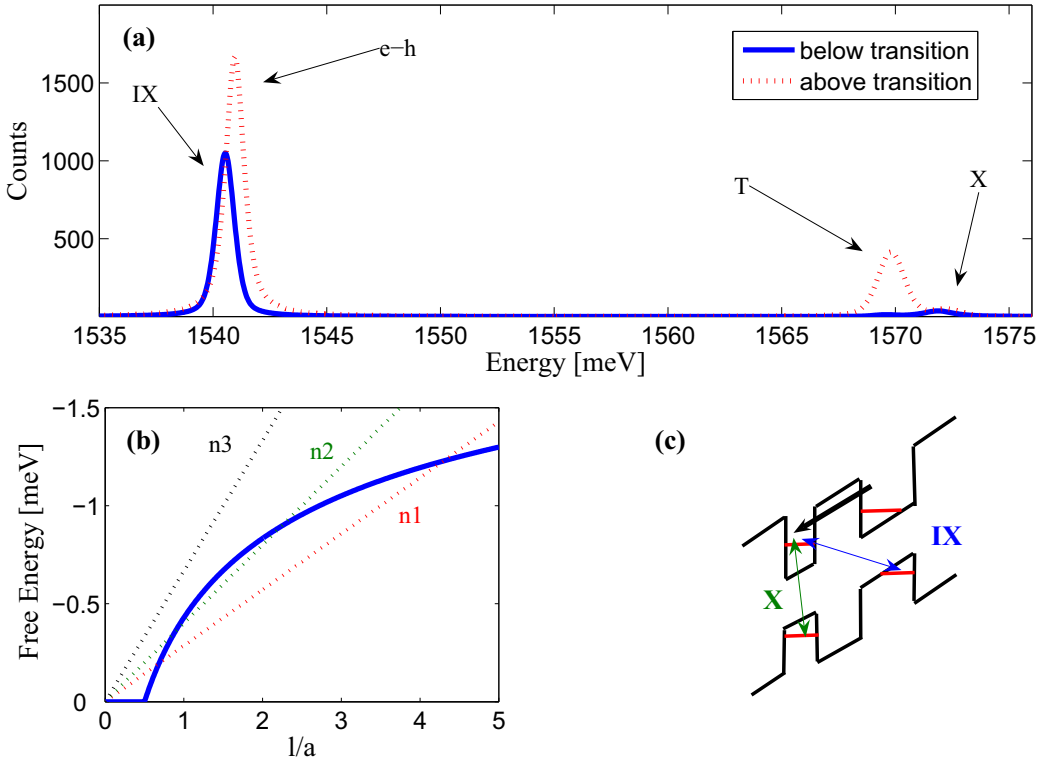

FIG. 4: (a) PL spectra below and above the transition showing the large increase in the T line above the transition. (b) The free energy of screened excitons (solid line) and electron-hole plasma (dashed lines) for different total pair densities as function of the screening length l. (c) Energy band diagram of the coupled quantum wells under perpendicular applied electric field showing the mixture of X and IX.

The authors would like to thank Y. Levinson, B. Laikhtman and D. Snoke for fruitful discussions. This research was supported by the Israeli Science Foundation and by the Scientific Cooperation Program of the French Embassy in Tel Aviv.

* Electronic address: mstern@weizmann.ac.il

[1] L.V. Keldysh, A.N. Kozlov, Soviet Phys. JETP, **27**, 521 (1968).

[2] N.F. Mott, Metal Insulator Transitions (Taylor and Francis, London, 1990).

[3] T.M. Rice *et al.*, The Electron Hole Liquid in Semiconductors (Solid State Phys., **32**, 1977).

[4] S. Ben Tabou de Leon, B. Laikhtman, Phys. Rev. B, **67**, 235315 (2003).

[5] S.W. Koch *et al.*, Phys. Stat. Sol. (b), **238**, 404 (2003).

[6] L. Kappei *et al.*, Phys. Rev. Lett., **94**, 147403 (2005).

[7] A. Amo *et al.*, J. Appl. Phys. **101**, 081717 (2007).

[8] J.E. Golub *et al.*, Phys. Rev. B, **41**, 8564 (1990).

[9] T. Fukuzawa, E.E. Mendez, and J.M. Hong, Phys. Rev. Lett., **64**, 3066 (1990).

[10] J.A. Kash *et al.*, Phys. Rev. Lett., **66**, 2247 (1991).

[11] V.B. Timofeev *et al.*, Phys. Rev. B, **61**, 8420 (2000).

[12] T.C. Damen *et al.*, Phys. Rev. B, **42**, 7434 (1990).

[13] D. Robart *et al.*, Solid State Commun., **95**, 287 (1995).

[14] H.X. Jiang *et al.*, Phys. Rev. B, **41**,12949 (1990).

[15] C. Piermarocchi *et al.*, Phys. Rev. B, **55**, 1333 (1997).

[16] S. Siggelkow *et al.*, Phys. Rev. B, **69**, 73104 (2004).

[17] L.V. Butov *et al.*, Nature, **417**, 47 (2002).

[18] D. Snoke *et al.*, Nature, **418**, 754 (2002).

[19] C.W. Lai *et al.*, Science, **303**, 503 (2004).

[20] S.I. Gubarev *et al.*,JETP Lett., **72**, 324 (2000).

[21] R. Zimmermann, C. Schindler, Solid State Commun., in press (2007)

[22] M. Bugajski, W. Kuzko and K. Reginski, Solid State Commun., **60**, 669 (1986).

[23] G. Finkelstein, H. Shtrikman and I. Bar-Joseph, Phys. Rev. Lett.,**74**, 976 (1995).

[24] I. Bar-Joseph, Semiconductor Science and Technology, **20**, 6R29 (2005).

2. Spatial manipulation of photo-excited carriers and excitons

An experiment in which the gas of excitons is explored in the immediate vicinity of the illumination spot is problematic in several respects. These include: local heating of the sample due to the illumination power which in effect prevents the attainability of the desired low lattice temperature, local current filaments causing hot electrons be injected into the QW near the illumination spot, which in turn deliver their excess energy to the exciton gas. Secondly, in this experiment the excitons are formed of initially hot photo-generated carriers. Then those hot excitons are assumed to equilibrate with the lattice within their lifetime. This demand would appear unnecessary if the carriers were prepared cold already before the exciton formation. This same situation was seemingly obtained in experiment by Yang et al. [21]. There the excitons formed on the boundary between the hole-rich and electron-rich regions. Interferometric examination of the light emanating from the recombined excitons revealed a strong enhancement of the coherence length below some temperature. This indicates that the gas of excitons thus obtained was cold. This experiment however lacks control of electron and hole densities and is not an efficient way of obtaining high density of excitons.

In this part we present some preliminary estimations and design details regarding the possible experimental setup in which the spatial control of the photogenerated particles can be conducted. The basic idea is: creation of excitons far from the region exposed to laser light having high density and low temperature. For this purpose we'll use various elements already tested experimentally as building blocks of the desired setup. The text is divided into subsections: first we present a flow chart describing the general idea, then main elements of the flowchart are examined separately, finally we describe how all these parts are combined in the proposed experiment and discuss some limitations imposed by semiconductor physics.

A schematic flowchart of the setup operation

Fig. 1 depicts a flowchart constituted of several blocks each describing a particular operation performed with the photoexcited carriers in coupled quantum wells. It can be divided into 4 stages. At each stage similar operation is done both on electrons and holes. At stage 1 carriers are photogenerated. At stage 2 they are

spatially separated by field ionization effect to obtain electron and hole gases at distinct nonoverlapping areas in the plane of the QWs. At stage 3 the carriers tunnel through the barrier between two coupled quantum wells driven by the out-of-plane electric field so the two gases appear separated in adjacent CQWs in addition to their separation *in the plane* of the QWs already obtained at the previous stage. At stage 4 the oppositely charged carriers diffuse over a macroscopic distance towards each other finally getting close enough so indirect excitons are formed somewhere at the midway. At stage 5 excitons recombine emitting light.

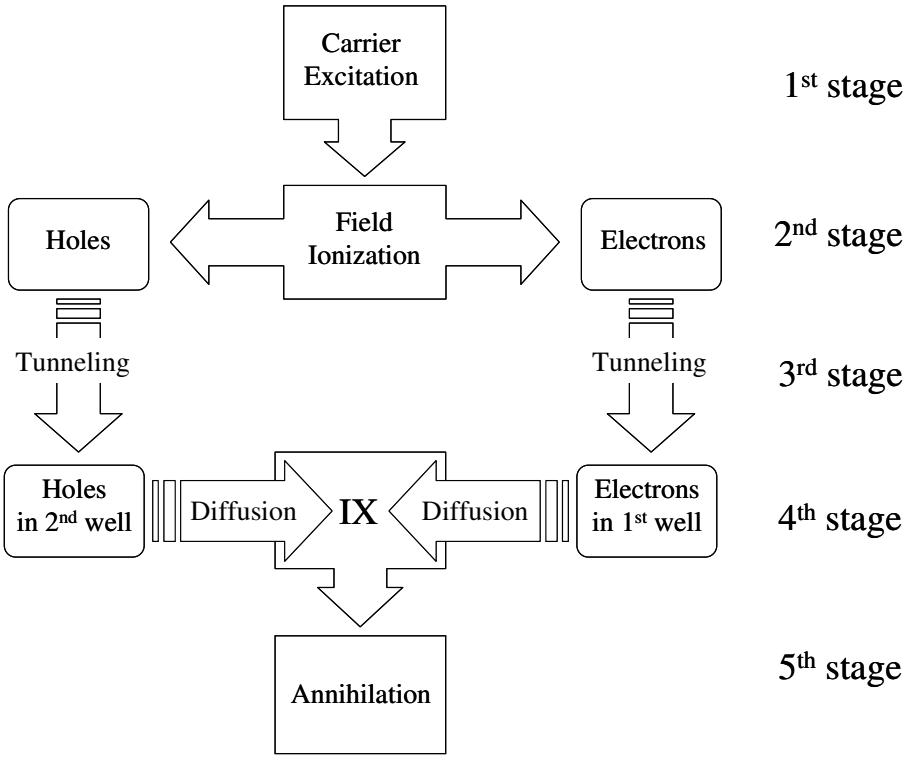

Fig 1: a flowchart of the device operation: 1st stage – carriers are generated by light. 2nd stage – electrons and holes are taken away from each other by strong in-plane electric field. 3rd stage – electrons and holes tunnel to adjacent QWs driven by out-of-plane electric field. 4th stage – electrons and holes being separated both in the plane and out of plane approach each other driven by diffusion over large distances and eventually form indirect excitons. 5th stage – excitons annihilate and emit light.

Second stage: Field ionization

Miller et al [18] have calculated the ionization rate of 2D excitons when electric field is applied parallel to the plane of the QW:

$$\frac{\Gamma}{Ry} = \frac{64}{\sqrt{\pi}} f^{-1/2} \exp\left(-\frac{32}{3f}\right) \quad (1)$$

Here $\Gamma = \hbar\omega$ is the ionization rate in energy units, Ry is the exciton Rydberg, f is the unitless in-plane electric field strength: $f = eF_{\parallel}a_B / Ry$, a_B being the exciton Bohr radius. This formula is summarized graphically in Fig. 2. Two main features are exhibited: the ionization rate is diminished for values of f below $f \sim 1.6$ which corresponds to field strength $F_{\parallel} \sim 1.6 \cdot Ry / ea_B$. This can be regarded as the ionization threshold. Starting from this value of f the rate rises nearly linearly.

In experiment the electric field is applied using metallic gates positioned on the sample surface. A simplest configuration of electrodes is sketched in Fig. 3a. Also the x-y-z coordinate axes are shown to simplify understanding. Two electrodes *A* and *B* are separated by a rectangular gap of width *w*. The lateral dimensions of the electrodes and the length of the gap are considered much larger than *w*.

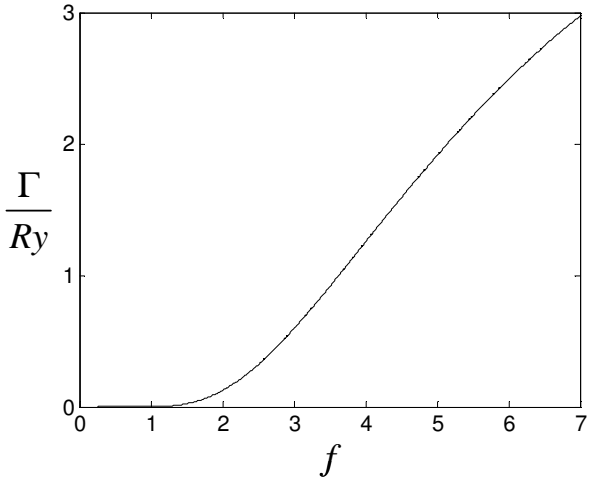

Fig 2: Normalized exciton field ionization rate vs. the applied lateral field

A third electrode is positioned on the back side of the sample at a depth D, so that the QWs appear sandwiched between the back electrode and the two top electrodes, namely *A* and *B*. In the appendix a simple technique is described by which the electric field components in the space between the electrodes can be calculated given the voltages supplied to each electrode. Consider $+1\text{V}$ is supplied to the right electrode, -1V to the left one, $w = 1\mu\text{m}$ and $D = 1\mu\text{m}$. In addition let's use the values $Ry = 4.2\text{meV}$ and $a_B = 14\text{nm}$ used in the paper by Miller [18], they are typical for direct excitons. The calculated spatial profile across the gap (x-direction) of the electric field projection on the *x* axis is shown in Fig. 3b for several depths (denoted by *d*) *below* the top electrodes. Obviously it vanishes for a depth equal to that of the back electrode (not shown on the figure) since only z-projection of the field must not vanish at the metallic plate surface and increases as the depth is reduced. The y-projection of the field vanishes everywhere due to the symmetry of the given geometry.

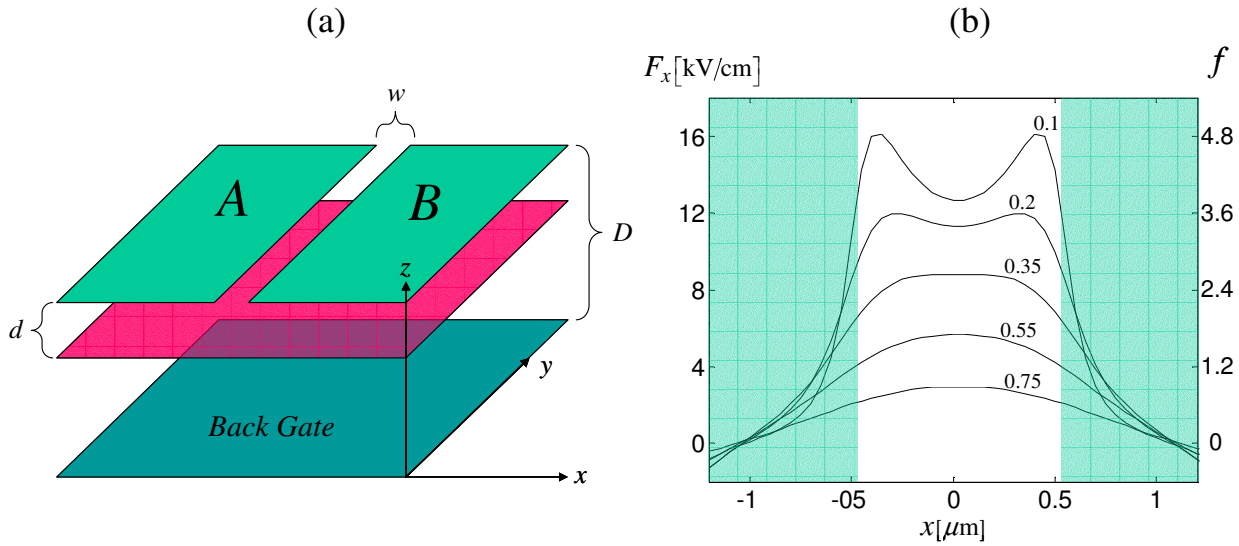

Fig 3: (a) A setup of electrodes where lateral electric field is induced with the parameters $w = 1\mu\text{m}$, $D = 1\mu\text{m}$. +1V and -1V are applied to the electrodes *A* and *B*. (b) x-component of the electric field for various values of *d* in μm. The green "curtains" mark the regions underneath the electrodes *A* and *B*.

Now, let's introduce illumination incident uniformly on the sample surface. The local exciton density $n(x,t)$ is evolving according to:

$$\frac{\partial n}{\partial t} = -\frac{n}{\tau} - \frac{n \cdot \Gamma(x)}{\hbar} + I \tag{2}$$

Here the first term on the RHS is the exciton recombination rate with τ being the exciton lifetime, the second term accounts for exciton field ionization with ionization rate depending on the local lateral electric field strength according to equation (1), *I* is the exciton creation rate due to the uniform illumination. For simplicity the diffusion of excitons is not accounted for. In the steady state regime $\partial n/\partial t = 0$, so we obtain the following expression for the total exciton density:

$$n(x) = I \cdot \left[\frac{1}{\tau} + \frac{\Gamma(x)}{\hbar} \right]^{-1} \tag{3}$$

Then, a number of *ionized* excitons per unit time per unit area is:

$$n_{ion}(x) = \frac{n(x)\Gamma(x)}{\hbar} = I \cdot \left[1 + \frac{\hbar}{\tau \cdot \Gamma(x)} \right]^{-1} \tag{4}$$

It follows that in locations where the ionization dominates over the radiative recombination, i.e. $\Gamma(x) \gg \hbar/\tau$, almost all the photogenerated excitons get ionized, while in the opposite limit $\Gamma(x) \ll \hbar/\tau$ the density of ionized excitons is proportional to the ionization rate: $n_{ion} \sim I\tau \cdot \Gamma(x)/\hbar$. In order to know how efficient the ionization due to the applied field is we integrate the expression for $n_{ion}(x)$ over the *x*-*y* plane and divide by total excitons generated in the gap between the electrodes:

$$P_{ion} = \frac{1}{w} \int dx \left[1 + \frac{\hbar}{\tau \cdot \Gamma(x)} \right]^{-1} \tag{5}$$

To set a quantitative estimate we must specify the value of the lifetime. Let it be 100ps, typical for direct excitons. The results of the calculation for several voltages supplied to the electrodes *A* and *B* and as a function of depth under the surface are presented in Fig. 4a. The most prominent feature reproduced for all voltages is the fast cut-off occurring at a specific depth (marked by an arrow for each voltage). Everywhere below this depth the field doesn't exceed the ionization threshold. It

suggests a way of obtaining effective ionization: simply position the QW well above the cut-off depth where the ionization is mostly efficient (the opposite goal of avoiding field ionization despite the applied voltage is reached by placing the QW deeper than the cutoff. This was utilized by Chen et al [17] in their X-trap). At a voltage of 0.1V the ionization vanishes entirely for any depth. Dividing this voltage by the gap width $w = 1\mu\text{m}$ we obtain typical field strength of 1kV/cm. This is below the estimated ionization threshold of 10kV/cm.

Important remark: although the exciton lifetime enters explicitly in the expression for the ionization efficiency, the latter appears to be almost insensitive to the lifetime value. In Fig. 4b two calculation results are shown at 0.5V, one for $\tau = 100\text{ps}$, the other for $\tau = 100\text{ns}$ (three orders of magnitude greater) typical for indirect excitons. Only insignificant differences appear. Therefore, one doesn't have to be concerned about the tunneling and relaxation dynamics in the CQWs in this context.

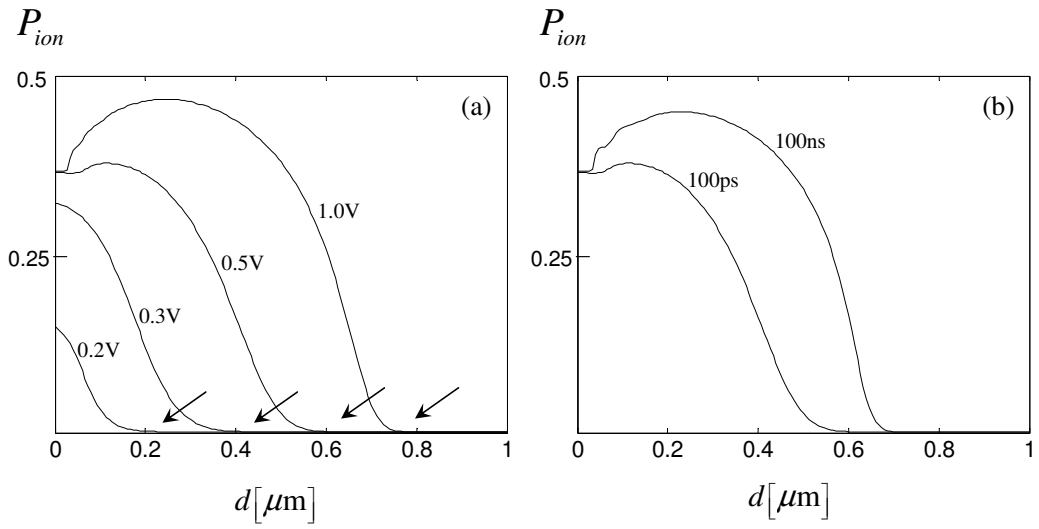

Fig. 4: Ionization efficiency under uniform illumination as a function of the depth *d* (see fig. 2 for setup details). (a) For various voltages on the electrodes *A* and *B*. Arrows point to the cutoff depths. (b) For two exciton lifetimes differing by three orders of magnitude.

Third stage: Tunneling

We should keep in mind the third dimension (out of the QWs plane) of the system. Ideally one would like to control the in-plane and the out-of-plane field components independently. At this stage the role of the back electrode becomes clear: a voltage difference between top and back electrodes and the distance between them are the parameters controlling mainly the out-of-plane component. If this distance is made much smaller than the lateral dimensions of the top electrodes, then a uniform electric field is induced underneath, except at the electrodes' boundaries. The out of plane field tilts the bands as was described in the introduction. By a proper choice of the voltage and its polarity the electron confinement energy in the wide well can be pushed above that in the narrow well. Then the electrons can tunnel from the wide well to the narrow well (see Fig. 1 in the introduction). In this same configuration the holes, generated in the narrow well, tunnel in the opposite direction i.e. to the wide well.

Fourth stage: Diffusion

Electrons or holes injected in the QWs underneath an equipotential electrode are free to diffuse in the lateral direction (*x* or *y* in Fig. 3a). We must take into account, however, the leakage of the carriers out of the QWs towards the metallic gates. This puts a limit on a distance from the excitation region over which appreciable carrier densities are sustained. This is dictated by the characteristic diffusion length given by $l = \sqrt{D\tau}$. Here *D* is the diffusion constant of the carriers, and τ is the typical time during which the carriers leak out, also called the storage time. Taking $D = 1\mathrm{cm}^2/\mathrm{sec}$ and $\tau = 100\mu\mathrm{sec}$ (reported for example by Kotthaus [19]), we obtain diffusion length of the order of $100\mu\mathrm{m}$. Therefore, the device of interest should have lateral dimensions comparable to this value.

The proposed setup

Now we have all the necessary ingredients at hand in order to explain the design of the experimental setup. A scheme of the top electrodes' design is depicted in Fig. 5. Three electrodes g1, g2, and g3 are defined on top of the substrate, so that all the gaps between them are as wide as one micrometer. Voltages of -3V, -2V and -1V (they can be varied of course) are applied on g1, g2 and g3 respectively relative to the back electrode (the minus sign will be explained in the next subsection). The light is incident in the spots s1 and s2 so that the gap between g1 and g2 is illuminated by s1 and the gap between g2 and g3 is illuminated by s2. In this configuration excitons ionize in s1 due to the in-plane field induced by a voltage difference between g1 and g2 in a way that the produced electrons are taken by the field to the left side of the electrode g2. By the same token holes produced in s2 accumulate on the right side of g2. The dynamics of carriers inside the CQWs is sketched on the right of Fig. 5. Notice the directions of the electric field in various sites of the setup. The field under g2 being oriented out-of-plane separates the two carrier gases namely electrons and holes in adjacent QWs due to tunneling. Nothing prevents from those electrons and holes under the equipotential electrode to diffuse towards each other, form excitons somewhere in the middle of g2 and eventually annihilate by emitting light. Those excitons are indirect since their very creation, for their constituent electrons and holes were separated in the two wells during their long diffusive motion. The two light spots can be separated by a distance up to the diffusion length which is typically hundred microns, assuring appreciable distance to the exciton creation region.

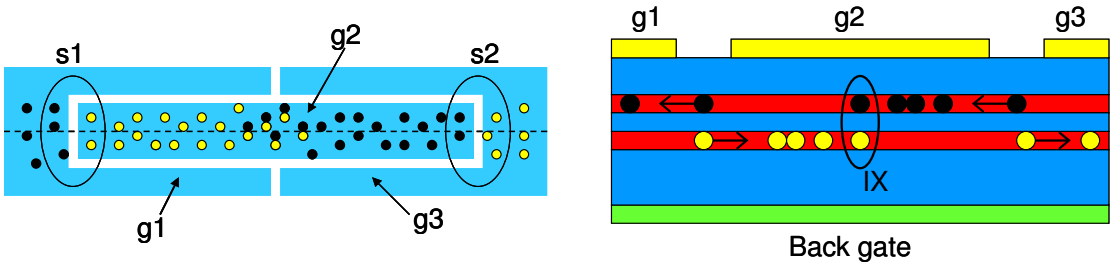

Fig 5: A design of a setup in which excitons are created away from the illumination regions. On the left: top view of the electrodes. On the right: a crossection along the dashed line demonstrating carrier motion in the CQW. Yellow and black circles are the electrons and holes respectively.

The densities of the two gases (i.e. electrons and holes) produced by field ionization can be controlled by varying the following parameters: the power of the incident illumination in spots s1 and s2 and the voltages on the top electrodes. The former defines a number of incident photons per unit time which in turn directly relates to the number of excitons a fraction of which is to be ionized. The latter controls the overall ionization rate (see Fig. 4a). It should be noted however, that at very high carrier densities the lateral field will be screened and, as a result, the ionization will be suppressed prohibiting further increase of the density, i.e. the device will be driven into saturation. The highest carrier densities which can be supported by a particular device depend on its geometry, storage time, and the voltages applied. We can estimate the saturation densities as follows: let's concentrate on regions far away from the gap between the electrodes say g1 and g2 (Fig. 6). There the field can be assumed uniform and aligned out-of-plane. Let V_1, V_2 be the voltages on the electrodes g1 and g2 respectively. Consider $V_1 < V_2$ so that holes produced by field ionization accumulate under g1 (let σ_h denote their charge density) and electrons correspondingly accumulate under g2 (let denote their charge density by σ_e). Assume all charge densities uniform. Now, let's calculate the work done on unity charge by the electric field on the path starting at the back electrode and ending at the top electrode for both g1 and g2. We divide the path into two consecutive segments: one going from the back electrode to the QW (distance $D-d$); the other going from the QW to the top electrode (distance *d*). The work done on the first segment is by definition the electrostatic potential on the QW. Thus the potentials V_1^{QW} and V_2^{QW} on the QW under g1 and g2 respectively:

$$V_1^{QW} = (D-d)\left(E_1 + \frac{2\pi}{\varepsilon}\sigma_h\right) \qquad 6)$$

$$V_2^{QW} = (D-d)\left(E_2 - \frac{2\pi}{\varepsilon}\sigma_e\right) \qquad 7)$$

Here E_1 and E_2 are the electric field contributions induced only by the charges on the electrodes in the regions under g1 and g2 respectively. The second terms in (6) and (7) in the far right brackets are the electric field contributions induced respectively by holes and electrons. The work done on the second segment being added to the potential on the QW is by definition the potential on the electrode. Therefore:

8) $$V_1^{QW} + d\left(E_1 - \frac{2\pi}{\varepsilon}\sigma_h\right) = V_1$$

9) $$V_2^{QW} + d\left(E_2 + \frac{2\pi}{\varepsilon}\sigma_e\right) = V_2$$

Note the signs in the brackets are opposite to those in (6-7) since now we are on the opposite side of the QW. From (6-9) we obtain:

10) $$\sigma_e + \sigma_h = \frac{\varepsilon}{4\pi d}\left[\Delta V - \left(1 - \frac{d}{D}\right)^{-1}\Delta V^{QW}\right]$$

Here $\Delta V \equiv V_2 - V_1$ and $\Delta V^{QW} \equiv V_2^{QW} - V_1^{QW}$ are the potential differences. The latter can be approximated by the typical in-plane field strength $E_{||}$ across the gap times the width of the gap w: $\Delta V^{QW} \approx E_{||} \cdot w$. When the lateral field strength $E_{||}$ drops below the ionization threshold because of screening, the density is saturated since the field ionization is diminished. The higher the voltage difference $V_2 - V_1$ or the smaller the depth d, the higher is the maximal attainable density. To roughly estimate the order of magnitude of maximal supported density let us neglect the second term in the square brackets and assume $\sigma_e = \sigma_h \equiv \sigma$. For typical values $\Delta V = 1\text{V}$, $\varepsilon \simeq 12$ (GaAs) and $d = 0.1\mu\text{m}$ we have: $\frac{\sigma}{e} \sim 5 \cdot 10^{11}\text{cm}^{-2}$.

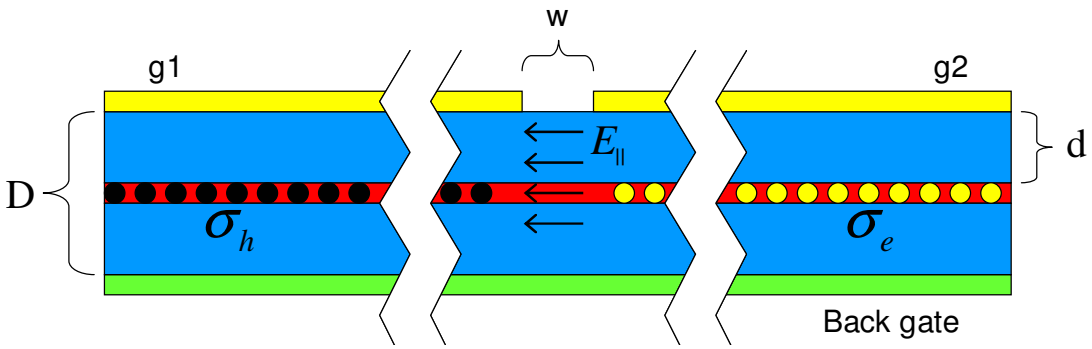

Fig. 6: Estimation of the saturation density. In the regions away from the gap w the out-of-plane electric field and the area densities of the holes and electrons are assumed uniform. Then knowing the voltages applied on the electrodes g1 and g2 one can estimate the maximal supported densities (see text).

The heterostructure

An important limitation which must be accounted for is dictated by the operation of our semiconductor device. A setup that we might use in our experiment is a heterostructure shown on the left of Fig. 7. On a GaAs substrate the following layers are grown: Si-doped GaAs serving as a conducting back electrode, AlGaAs barrier, two GaAs Quantum wells separated by AlGaAs tunneling barrier, and finally AlGaAs capping. On the surface a metallic film is evaporated being the top electrode. Notice the relatively close proximity of the QWs to the top surface. There the field ionization is mostly effective as was described earlier (the QWs are placed well above the cut-off depth). On the right of Fig. 7 the conduction band of the structure is shown. On the highly doped contact layer at the bottom of the sample the conduction band is pinned to the Fermi level. On the top side, at the interface with a metal, the conduction band is half a gap above the Fermi level, which is around 0.75eV. Hence a built-in field is formed inside with no voltage applied between top and back electrodes. This field can be compensated over and even reversed in direction by applying positive voltage relative to the back electrode. But in this case a strong flow of electrons will be conducted from the back electrode. This is the forward bias operation.

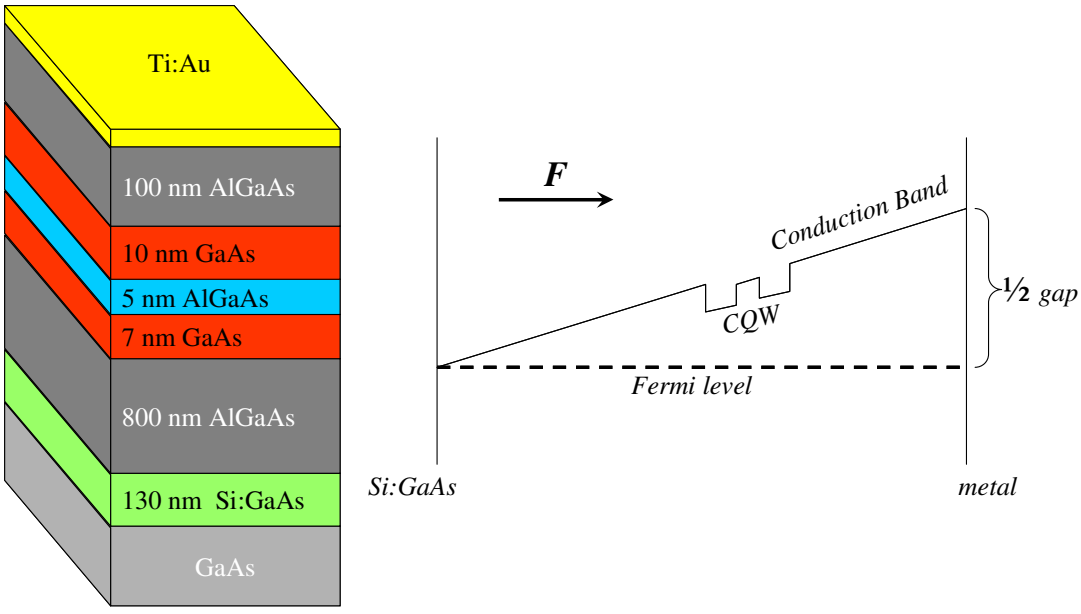

Fig 7: On the left is the heterostructure design. On the right is its band diagram.

We don’t want our device to work in this mode since the high current can disturb our experiments. On the other hand when a negative voltage is applied to the top electrode the Schottky barrier prevents the flow of electrons from the top electrode. This is the reversed bias. In this mode the device is much like a capacitor with a dielectric insulator sandwiched between two metallic plates. It than follows, that we are limited to operate our device in reversed bias mode only.

Appendix: calculation of electrostatic field induced by metallic gates

The described method is limited for a configuration sketched in Fig. 1. Consider flat electrodes of arbitrary shape positioned on the boundary between two dielectrics with dielectric constants ε_1 and ε_2. A third electrode covers the whole area on the back side of dielectric ε_1. Now voltages are applied to the disconnected top electrodes relative to the back electrode. It follows from image charge method [20] that the electric field in the space between the top and back electrodes doesn't depend on ε_1 or ε_2, only the charge density accumulated on the top electrodes is directly proportional to their arithmetic mean $(\varepsilon_1 + \varepsilon_2)/2$. Therefore the calculation will be conducted assuming $\varepsilon_1 = \varepsilon_2 = 1$ without losing a generality. Instead of solving the Poisson equation given the boundary conditions defined by the potentials on the electrodes we approach the problem as follows: consider a rectangular grid of point charges filling a domain defined by electrodes' geometrical shapes (Fig.2 left). A copy of this grid with no charges is placed at a distance *d* below (Fig 2 right). On the points of this latter grid we define potentials so that within a domain of particular electrode's shape all the potentials are set equal to the voltage applied on the corresponding electrode. The main task is to calculate those values of the point charges that induce these potentials on the copied grid. Let's denote the charges by q_i and the potentials by v_i, where the subindex runs over the grid. First assume the back electrode is absent so that both dielectrics are semi-infinite. Then we have the relations: $v_i = \sum_j q_j / r_{ij}$. Here r_{ij} is the distance between the charge q_j and the *i*-th site on the copied grid. Now the problem is reduced to algebraic solution of a system of linear equations: given the potentials we solve for the unknown charges. Once the charges are found, we use their values to calculate the electric field components at arbitrary location by the formula $\vec{E} = \sum_i q_i \cdot \vec{r_i} / r_i^3$, where $\vec{r_i}$ is the vector connecting between the charge q_i and the given location. Now let's introduce the back electrode at a distance *D* below the point charges' grid. Using the image charges method we place a charge $-q_i$ against a respective charge q_i on the opposite side of the back

electrode and at a distance D from it. The necessary modifications are straightforward: replace the above formulas by

$$v_i = \sum_j q_j \left(\frac{1}{r_{ij}} - \frac{1}{r'_{ij}} \right),$$

$$\vec{E} = \sum_i q_i \left(\frac{\vec{r}_i}{r_i^3} - \frac{\vec{r}'_i}{r'^3_i} \right)$$

Here the primed r denotes the distance to the image charge.

The calculation is accurate when the grid constant and the distance d are set appreciably smaller than typical smallest dimensions in the setup.

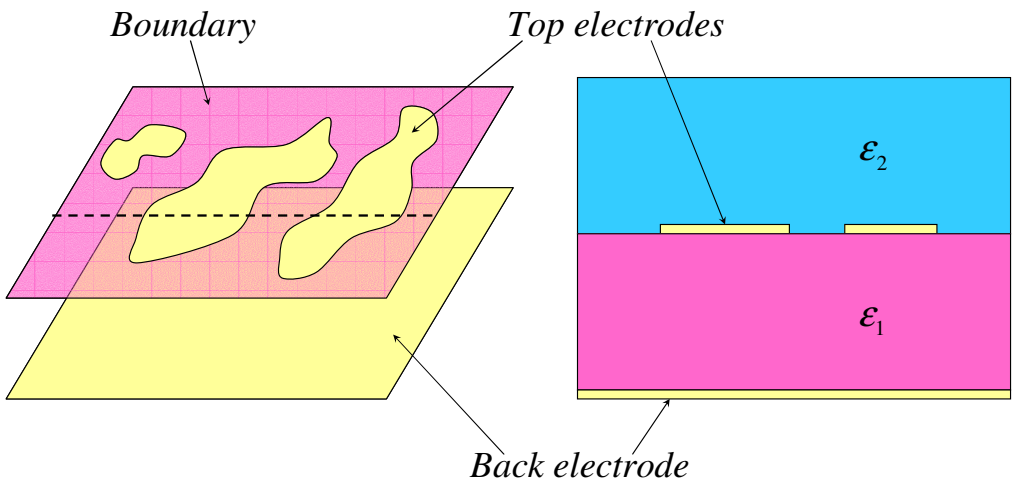

Fig. 1: Most general geometry for which the method is applicable. On the right is the crossection along a dashed line shown on the left

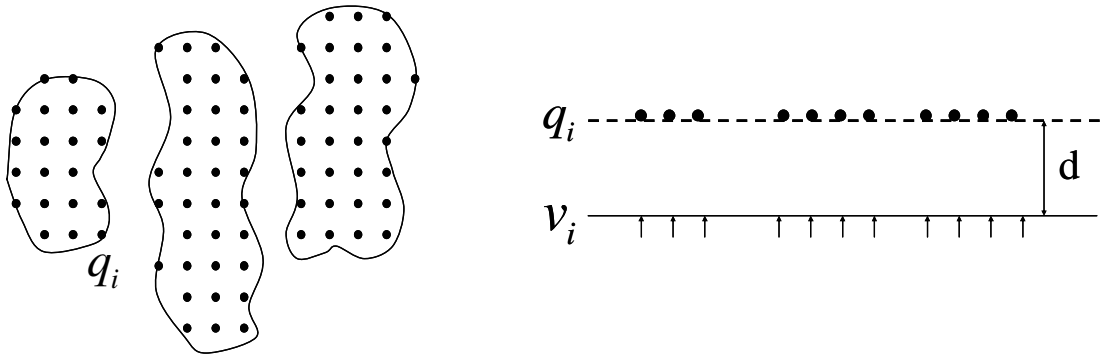

Fig. 2: Method description. On the left: point charges on a grid, top view. On the right: a cross section. Small arrows are pointing to the sites where potentials are defined. Small circles are the point charges a distance d above.

Conclusions

The Mott transition of exciton in coupled quantum wells

We were able to distinguish between the two phases, i.e. excitonic and electron-hole plasma by both spectroscopic means and measurements in a magnetic field. We showed that the transition occurs abruptly at a certain critical exciton density and temperature. We established a density-temperature phase diagram and confirmed that the transition is thermodynamic. The observed transition is shown to be driven by the existence of direct excitons in the system, which enables the occurrence of the transition.

Spatial manipulation of photoexcited carriers and excitons

In this part a scheme of spatial manipulation of photo-excited particles was examined. In the experimental realization the excitons are to be created at a macroscopic distance away from the illuminated region. We performed necessary preliminary calculations and showed that this can be implemented in principle by a dissociation of excitons in the illumination region utilizing the field ionization effect and their subsequent composition in a remote location.

References

[1] Y. J. Chen et al., Phys. Rev. B, 36, 4562 (1987)

[2] T. Fukuzawa et al., J. Quant. Elect., 26, 811 (1990)

[3] A. Alexandrou et al. Phys. Rev. B, 42, 9225 (1990)

[4] J. M. Kosterlitz, D. J. Thouless, J. Phys. C, 6, 1181 (1973)

[5] G. Schmid et al., Phys. Rev. Lett., 88, 167208 (2002)

[6] N. F. Mott, Philos. Mag., 6, 287 (1961)

[7] L. M. Smith, J. P. Wolfe, Phys. Rev. Lett., 57, 2314 (1986)

[8] L. Kappei et al., Phys. Rev. Lett., 94, 147403 (2005)

[9] A. Amo et al., J. Appl. Phys., 101, 081717 (2007)

[10] V. B. Timofeev et al., Phys. Rev. B, 61, 8420 (2000)

[11] S. Ben-Tabou, B. Laikhtman, Phys. Rev. B, 67, 235315 (2003)

[12] S. W. Koch, Phys. Stat. Sol. (b), 238, 404 (2003)

[13] V. Bagnato, D. Kleppner, Phys. Rev. A, 44, 7439 (1991)

[14] V. Negoita, D. W. Snoke et al., Appl. Phys. Lett., 75, 2059 (1999)

[15] R. B. Balili, D. W. Snoke, Appl. Phys. Lett., 88, 031110 (2006)

[16] A. T. Hammack et al., J. Appl. Phys., 99, 066104 (2006)

[17] G. Chen, et al., Phys. Rev. B., 74, 045309 (2006)

[18] D. A. B. Miller et al, Phys. Rev. B, 32, 1043 (1985)

[19] J. P. Kotthaus et al., Phys. Stat. Sol. (b), 243, 14, 3754 (2006)

[20] J. D. Jackson, *Classical Electrodynamics*, John Wiley & Sons, Inc. (1962)

[21] Sen Yang et al., Phys. Rev. Lett., 97, 187402 (2006)